**SAINSTEK: JURNAL SAINS DAN TEKNOLOGI**
Publisher: Universitas Islam Negeri Mahmud Yunus Batusangkar
Website: https://ejournal.uinmybatusangkar.ac.id/ojs/index.php/sainstek
E-mail: sainstek@uinmybatusangkar.ac.id

June 2026
Vol 18 No 1
ISSN: 2085-8019 (p)
ISSN: 2580-278X (e)
pp : 89-97

# DFT+U Investigation of Electronic Properties of $CuO/Fe_2O_3$ Heterojunction: Band Gap Engineering and Charge Transfer Mechanism for Photocatalytic Water Splitting

**Maulana Reizqy Anughrah, Riri Jonuarti*, Leni Azius Fitri, Eka Susanti**
*Department of Physics, Universitas Negeri Padang,*
*Jln. Prof. Dr. Hamka, Air Tawar Barat, Kecamatan Padang Utara, Kota Padang, Sumatera Barat, Indonesia*
*email: riri_jonuarti@fmipa.unp.ac.id*

**Article History**
Received: 24 June 2026
Reviewed: 27 June 2026
Accepted: 30 June 2026
Published: 30 June 2026

**Keywords**
DFT+U; $\alpha - Fe_2O_3$; $CuO/Fe_2O_3$ heterojunction; band-gap engineering; S-scheme; water splitting

**Abstract**
The development of efficient, earth-abundant photocatalysts for solar water splitting remains a central challenge in renewable-energy research. The electronic properties of $\alpha - Fe_2O_3$, a $CuO/Fe_2O_3$ heterojunction, and the adsorption of water-derived species on the $\alpha - Fe_2O_3$ surface were investigated using spin-polarized first-principles calculations within the DFT+U framework, as implemented in the Vienna Ab initio Simulation Package (VASP) with the GGA-PBE functional and Hubbard corrections of U = 5.3 eV (Fe-3d) and U=6.5 eV (Cu-3d). The pristine $\alpha - Fe_2O_3$ slab exhibits an indirect band gap of 1.28 eV, with the valence band maximum (VBM) at Γ and the conduction band minimum (CBM) between Y and Γ; the valence band is dominated by O-2p states and the conduction band by Fe-3d states, while symmetric spin channels confirm its antiferromagnetic character. Formation of the $CuO/Fe_2O_3$ heterojunction widens the indirect gap to 1.61 eV (Δ= +0.33 eV), driven by hybridization of Cu-3d and Fe-3d orbitals that lifts the lower conduction band, with empty Cu-s states appearing near 2.8 eV above the Fermi level. The orbital redistribution is suggestive of an S-scheme charge-transfer mechanism in which CuO acts as the reduction photocatalyst and $Fe_2O_3$ as the oxidation photocatalyst. Among the adsorbed species, the interaction strength increases in the order $H_2O$ < •$OH$ < •$OOH$, with •$OOH$ showing the strongest Fe–O orbital hybridization. The gap remains below experimental value (≈2.1 eV). These results point to $CuO/Fe_2O_3$ as candidate visible-light S-scheme photocatalyst for the oxygen evolution reaction, while a quantitative assessment of the reaction is left for future work.

## INTRODUCTION

Rising global energy demand and the urgent need to move beyond fossil fuels have intensified the search for clean, storable energy carriers. Photocatalytic water splitting, in which a semiconductor uses solar photons to drive the decomposition of water into hydrogen and oxygen, offers an attractive route to carbon-free fuel (Alamgir et al., 2025). Since the

demonstration of photoelectrochemical water splitting, sustained effort has focused on identifying stable (Fujishima & Honda, 1972), inexpensive and visible-light-active semiconductors able to carry out the hydrogen evolution reaction (HER) and the oxygen evolution reaction (OER) with high efficiency (Guo et al., 2026).

Among candidate photoanode materials, $\alpha - Fe_2O_3$ (hematite) is especially attractive because it is earth-abundant, non-toxic, chemically stable in aqueous media and inexpensive. Its experimental optical gap of about 2.1 eV permits absorption over much of the visible spectrum (Sivula et al., 2011). In practice, however, the performance of hematite is limited by rapid recombination of photogenerated carriers, a very short hole-diffusion length and sluggish surface OER kinetics, all of which suppress its solar-to-hydrogen efficiency (Gao et al., 2023).

Copper(II) oxide (CuO) is a p-type semiconductor with a narrow experimental band gap near 1.5 eV (Kyesmen et al., 2021), which makes it an effective visible-light absorber that complements hematite. Used on its own, however, CuO suffers from limited photochemical stability and modest efficiency. Coupling p-type CuO with n-type hematite to form a heterojunction is therefore a natural strategy for combining their favourable optical properties while mitigating their individual weaknesses (Nallapureddy et al., 2025) .

Constructing a $CuO/Fe_2O_3$ composite establishes an internal electric field at the interface that promotes spatial separation of photogenerated electrons and holes. When the two oxides are arranged with staggered band edges, charge transfer can follow a step-scheme (S-scheme) pathway, in which CuO serves as the reduction photocatalyst and $Fe_2O_3$ as the oxidation photocatalyst (Lv et al., 2025). Unlike a conventional type-II junction, the S-scheme preferentially recombines the less energetic carriers while preserving the strongly reducing electrons and strongly oxidizing holes, thereby maximizing the redox driving force (Low et al., 2017).

Experimentally, $CuO/Fe_2O_3$ heterostructures show enhanced photoelectrochemical water-splitting activity relative to bare hematite (Kyesmen et al., 2021). Although many experimental studies have addressed $CuO/Fe_2O_3$ composites, the atomistic origin of the band-gap modification and the charge-transfer mechanism remains incompletely understood. First-principles modelling is well suited to this problem, but standard semilocal functionals such as GGA-PBE severely underestimate the band gaps of transition-metal oxides because of the self-interaction error associated with the localized Fe-3d and Cu-3d electrons (Huang et al., 2016). The Hubbard-corrected DFT+U approach partially restores a correct description of these correlated states, yet systematic DFT+U studies of $CuO/Fe_2O_3$ heterojunctions are still scarce (Naveas et al., 2023). Specifically, how the band-edge positions and orbital character of $CuO/Fe_2O_3$ are altered relative to pristine hematite, and how this orbital redistribution relates to a candidate S-scheme charge-transfer pathway, have not been resolved at the DFT+U level for this composite. The present work therefore employs spin-polarized DFT+U calculations to investigate (i) the electronic structure of the pristine $\alpha - Fe_2O_3$ slab, (ii) the band-gap engineering and charge-transfer behaviour of the $CuO/Fe_2O_3$ composite, and (iii) the adsorption of the OER intermediates $H_2O$, $\bullet OH$ and $\bullet OOH$ on the hematite surface, in order to clarify the potential of $CuO/Fe_2O_3$ as an S-scheme photocatalyst for water splitting.

## METHOD

All calculations were carried out using spin-polarized density functional theory (DFT) as implemented in the Vienna Ab initio Simulation Package (VASP) version 5.4.4 (Kresse & Hafner, 1993). Electron–ion interactions were described with the projector augmented-wave (PAW) method (Blöchl, 1994), and exchange–correlation effects with the generalized gradient approximation in the Perdew–Burke–Ernzerhof (GGA-PBE) form (Perdew et al., 1996). To correct the self-interaction error of the localized d electrons, the rotationally invariant DFT+U scheme of Dudarev (LDAUTYPE = 2) was applied (Dudarev & Botton, 1998).

$$E_{\mathrm{DFT+U}} = E_{\mathrm{DFT}} + \frac{U-J}{2}\sum_{\sigma}\left[\mathrm{Tr}(n^{\sigma}) - \mathrm{Tr}(n^{\sigma}n^{\sigma})\right]$$

$$U_{\text{eff}} = U - J$$

with effective Hubbard parameters U = 5.3 eV for Fe-3d and U = 6.5 eV for Cu-3d (Naveas et al., 2023).

A plane-wave kinetic-energy cutoff (ENCUT) of 520 eV was used, and the Brillouin zone of the two-dimensional periodic slab was sampled with a Γ-centered 3×3×1 k-point mesh (Monkhorst & Pack, 1976). Electronic self-consistency was converged to $1\times10^{-6}$ eV (EDIFF), and ionic relaxation was stopped once residual forces fell below 0.02 eV/Å (EDIFFG = −0.02 eV/Å). Gaussian smearing (ISMEAR = 0) with a width of σ = 0.05 eV was applied. To stabilize convergence of the antiferromagnetic (AFM) state, the mixing parameters AMIX = 0.2 and BMIX = 0.0001 were used, and the AFM order of hematite was imposed through the initial magnetic moments (MAGMOM), with Fe moments arranged as 5×5.0, 5×−5.0, 6×5.0 μB.

The $\alpha - Fe_2O_3(\bar{1}02)$ surface, one of the most thermodynamically stable hematite terminations, was adopted as the slab model (Tanwar et al., 2007). A vacuum spacing of at least 20 Å was inserted along the surface normal to remove spurious interactions between periodic images (Hofmann et al., 2021). Selective dynamics were employed: the bottom atomic layers were frozen (F F F) to mimic the bulk, while the topmost layers and the adsorbates were fully relaxed (T T T). The $CuO/Fe_2O_3$ composite was modelled by bringing CuO units into contact with the hematite slab to form an interface.

To probe the OER, the intermediates $H_2O$, $\bullet OH$ and $\bullet OOH$ were adsorbed individually at the coordinatively unsaturated surface iron (Fe-top) site. After relaxation, band structures along the high-symmetry k-path together with the total and projected densities of states (DOS and PDOS) were extracted and post-processed using the VASPKIT package (Wang et al., 2021). The band-gap type and the orbital character of the VBM and CBM were identified from the PDOS, and the strength of the surface interactions was assessed from the energy shifts and broadening of the Fe-3d, O-2p and H-s projections. The main computasional paramters use in this study are summarize on Table 1.

Table 1. Main Computational Parameters Used in the DFT+U Calculations.

| Parameter | Value / setting |
|---|---|
| Software | VASP v5.4.4 |
| Pseudopotential | PAW |
| Exchange–correlation functional | GGA-PBE |
| Hubbard correction | DFT+U, Dudarev (LDAUTYPE = 2) |
| U (Fe-3d) / U (Cu-3d) | 5.3 eV / 6.5 eV |
| Plane-wave cutoff (ENCUT) | 520 eV |
| k-point mesh | Γ-centered 3×3×1 |
| Energy convergence (EDIFF) | $1\times10^{-6}$ eV |
| Force convergence (EDIFFG) | −0.02 eV/Å |
| Smearing (ISMEAR) | Gaussian, σ = 0.05 eV |
| Spin polarization (ISPIN) | 2 (spin-polarized, AFM) |
| Surface model | $\alpha - Fe_2O_3(\bar{1}02)$, vacuum ≥ 20 Å |

## RESULT AND DISCUSSION

### *Electronic Structure of the $\alpha - Fe_2O_3$ Slab*

$$E_g = E_{\text{CBM}} - E_{\text{VBM}}$$

Note: $E_{CBM}$ conduction band minimum energy; $E_{VBM}$ valence band maximum energy. The gap is indirect if both are at different k-points

The calculated band structure of the pristine $\alpha - Fe_2O_3$ slab is shown in Fig 1a. The material behaves as a semiconductor with an indirect band gap of 1.28 eV: the VBM is located at the Γ point (0,0,0), whereas the CBM lies along the path between Y and Γ. Because the band extrema occur at different k-points, transitions across the gap are indirect and require phonon assistance, consistent with the optical behaviour of hematite. The Fermi level lies within the gap, confirming the semiconducting character.

The orbital composition is revealed by the PDOS (Fig. 1c). The upper valence band, extending from about −1 to −6 eV below the

Fermi level, is dominated by O-2p states, while the lower conduction band, between roughly 1.3 and 2.5 eV, is governed by Fe-3d states. This O-2p → Fe-3d character of the fundamental transition is typical of charge-transfer-type transition-metal oxides. The spin-up and spin-down channels of the total DOS are essentially symmetric (Fig. 1b), giving zero net magnetization, fully consistent with the antiferromagnetic ground state imposed through the MAGMOM setting.

The computed gap of 1.28 eV (1.29 eV from the PDOS) is smaller than the experimental optical gap of ≈2.1 eV. This underestimation is expected: even with a Hubbard correction, GGA+U tends to place the gap of hematite within the broad 1.0–2.2 eV range reported in the literature (Naveas et al., 2023), reflecting the residual self-interaction error of semilocal functionals and the sensitivity of the gap to the chosen U value, surface termination and slab thickness. Despite this quantitative offset, the qualitative picture—an indirect, O-2p/Fe-3d gap with antiferromagnetic order—is robust and provides a reliable reference for analysing the composite.

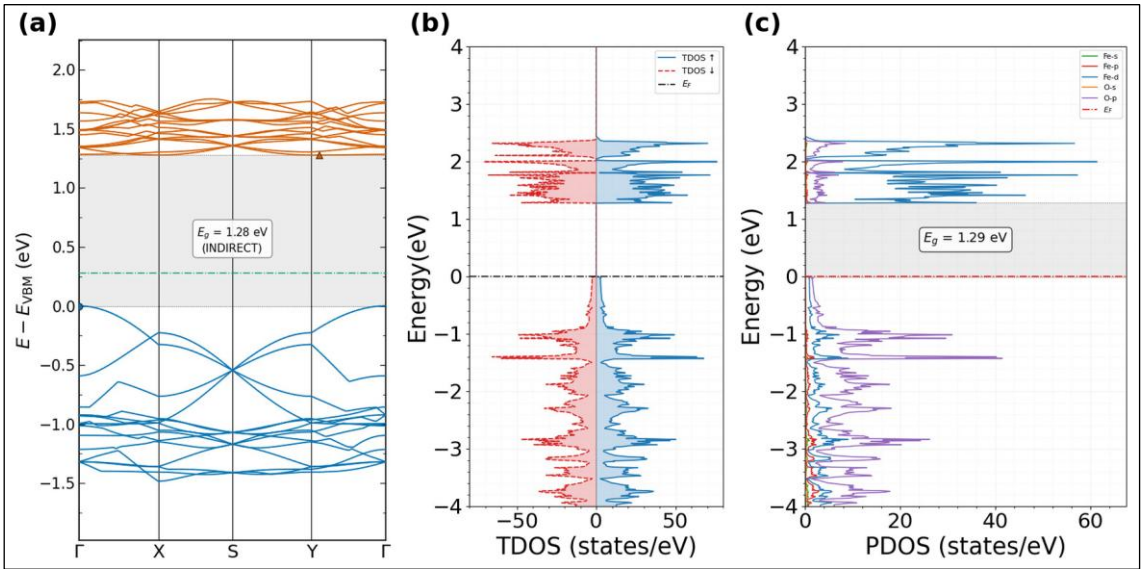


Figure 1. Electronic structure of the pristine $\alpha - Fe_2O_3$ slab: (a) band structure along Γ–X–S–Y–Γ with an indirect gap of 1.28 eV; (b) spin-resolved total density of states (TDOS); (c) projected density of states (PDOS). The symmetric spin-up/spin-down channels in (b) confirm the antiferromagnetic ground state, and the valence and conduction bands are dominated by O-2p and Fe-3d states, respectively.

### *Electronic Structure of the $CuO/Fe_2O_3$ Composite*

Upon formation of the $CuO/Fe_2O_3$ heterojunction, the indirect band gap increases from 1.28 to 1.61 eV, an upward shift of +0.33 eV (Figs. 1 and 2). The PDOS yields a gap of 1.61 eV (Fig. 2c), and the band structure gives a consistent indirect gap of 1.59 eV (Fig. 2a); the small difference reflects the k-mesh and DOS-grid resolution. The gap remains indirect, so the heterojunction retains phonon-assisted absorption. A wider gap does not by itself improve visible-ligth harvestin, widening the gap can in principle narrow arbsorbate spectral rang. However, 1.67 eV still corresponds to a photon wavelegength of about 770 nm, well within the visible range, so the gap increases reported here is not expexted to compromise visible-light absorption. A definitive assessment would require computing the optical absorption spectrum and the absolute band-edge positions relative to the redox potentials of water, which is left for future work (Walter et al., 2010).

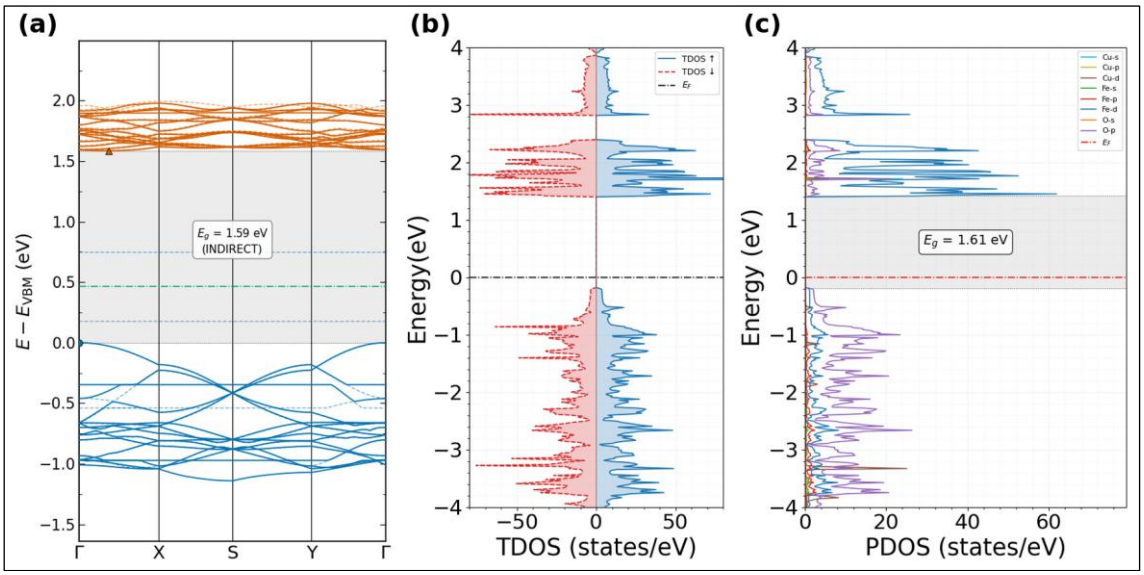


Figure 2. Electronic Structure of the $CuO/Fe_2O_3$ Composite: (a) Band Structure with an Indirect Gap of 1.59 eV; (b) spin-resolved TDOS; (c) PDOS with a Gap of 1.61 eV, Showing Hybridization of Cu-3d and Fe-3d States in the Conduction Band and Empty Cu-s states near 2.8 eV above the Fermi Level.

Analysis of the composite PDOS clarifies the origin of this widening (Fig. 2c). The lower conduction band now arises from hybridization between Cu-3d and Fe-3d states: mixing of the two metal d manifolds pushes the effective CBM to higher energy, which directly accounts for the larger gap. In addition, empty Cu-s states appear approximately 2.8 eV above the Fermi level, contributing to the upper conduction band and marking the unoccupied Cu-derived levels. The valence band continues to be dominated by O-2p states, now with an additional Cu-3d contribution, indicating electronic coupling between the CuO and $Fe_2O_3$ components across the interface. The overall shift of the composite PDOS relative to pristine hematite is direct evidence of interfacial electronic interaction rather than a simple physical mixture. The resulting band-edge alignment and orbital character are summarized schematically in Fig 3.

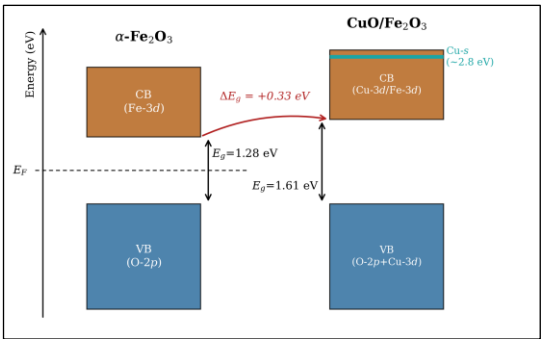


Figure 3. Schematic band-edge Diagram Illustrating the band-gap Engineering of $CuO/Fe_2O_3$ (1.28 → 1.61 eV) and the Orbital Character of the Band Edges.

These features are compatible with, and suggestion of, an S-scheme charge-transfer mechanism (Fig. 4), although this assignment is based on orbital hybridization and DOS analysis alone, explicit confirmation would require band-alignment, work-function, and charge-density-different calculation, which are recommended for future work. In this picture CuO, with its more negative conduction band, acts as the reduction photocatalyst (RP), while $Fe_2O_3$, with its more positive valence band, acts as the oxidation photocatalyst (OP) (Xu et al., 2020).

Under illumination, the internal electric field and band bending at the interface drive recombination of the less energetic electrons in the $Fe_2O_3$ conduction band with the holes in the CuO valence band, leaving strongly reducing electrons in the CuO conduction band and strongly oxidizing holes in the $Fe_2O_3$ valence band (Jiang et al., 2023). This spatial separation enhances simultaneous reduction and oxidation while suppressing bulk recombination. Importantly, a gap of 1.61 eV remains within the visible range, so the improved charge separation is achieved without sacrificing light absorption—a key requirement for an efficient water-splitting photocatalyst.

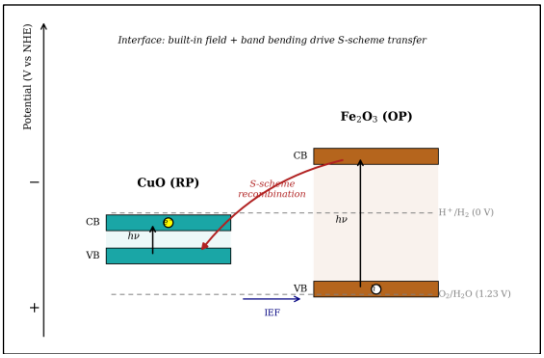


Figure 4. Proposed S-scheme Charge-Transfer Mechanism at the $CuO/Fe_2O_3$ Interface, with CuO as the Reduction Photocatalyst (RP) and $Fe_2O_3$ as the Oxidation Photocatalyst (OP).

***Adsorption of Water Species on the $\alpha - Fe_2O_3$ Surface***

The OER proceeds through a sequence of surface intermediates, conventionally $H_2O \rightarrow \bullet OH \rightarrow \bullet OOH \rightarrow O_2$. To assess how strongly each intermediate binds to hematite, $H_2O$, $\bullet OH$ and $\bullet OOH$ were adsorbed at the surface Fe-top site, and the resulting PDOS were compared with that of the clean surface (Fig. 5) (Nørskov et al., 2004).

For adsorbed $H_2O$ (Fig. 5a), the molecular O-2p states appear in the −1 to −3 eV region and the H-s contribution below the Fermi level is small, while the surface Fe-3d profile shifts only slightly to lower energy relative to the clean slab. Together these features indicate a comparatively weak, largely physical interaction with weak O–H related coupling.

For the $\bullet OH$ radical (Fig. 5b), the O-2p states move closer to the Fermi level than in the $H_2O$ case, and the surface Fe-3d states also shift toward the Fermi level. The reduced PDOS gap signals a stronger, more chemical interaction between $OH$ and the surface Fe atom than for water.

For $\bullet OOH$ (Fig. 5c), the PDOS displays two O-2p peaks, reflecting the two inequivalent oxygen atoms of the $OOH$ group, while the Fe-3d states become noticeably broadened; a small H-s contribution is detected near −2.5 eV. The broad Fe-3d distribution indicates strong Fe–O orbital hybridization and a coordinative bond, characteristic of chemisorption at the Fe-top site.

To complement the PDOS analysis, the relaxed Fe–O bond distances at the adsorption sites were examined as a structural indicator of the interaction strength. The Fe–O distances decreased significantly, from 2.26 Å for cap H ₂ cap O to a range of 1.83–1.84 Å for •OH and •OOH . The complete thermodynamic ranking via adsorption energies (E_ads = E(slab adsorbate) − E(slab) − E(adsorbate, gas)) was not calculated in this study due to limited computational resources, and is recommended as a direction for future work.

The three adsorbates therefore follow a clear order of increasing interaction strength, $H_2O < \bullet OH < \bullet OOH$ (Table 2). The pronounced broadening of the Fe-3d states upon $\bullet OOH$ adsorption is consistent with a more reactive OER intermediate and supports facile $O_2$ formation as the final OER product. The strong, selective binding of $\bullet OOH$ at the hematite surface complements the improved charge separation of the $CuO/Fe_2O_3$ junction, suggesting that the composite can both generate and deliver the carriers required to drive water oxidation. The trend $H_2O < \bullet OH < \bullet OOH$ obtained here is qualitatively consistent with the binding-strength ordering reported for OER intermediates on Fe-based oxide surfaces in the

computational hydrogen-electrode framework of (Nørskov et al., 2004), where absorption strengthens as radical character od intermediate increases. A quantitative comparison with the absorption-energy and overpotential values reported in such studies was not possible in this work because the gas-phase reference energy required for $E_{ads}$= E (slap adsorbate)- E (slap) – E (absorbate, gas ) could not be obtained, this calculation, together with the reaction-thermodynamic analysis needed to evaluated the OER over potential, is identified as a priority for follow-up the work.

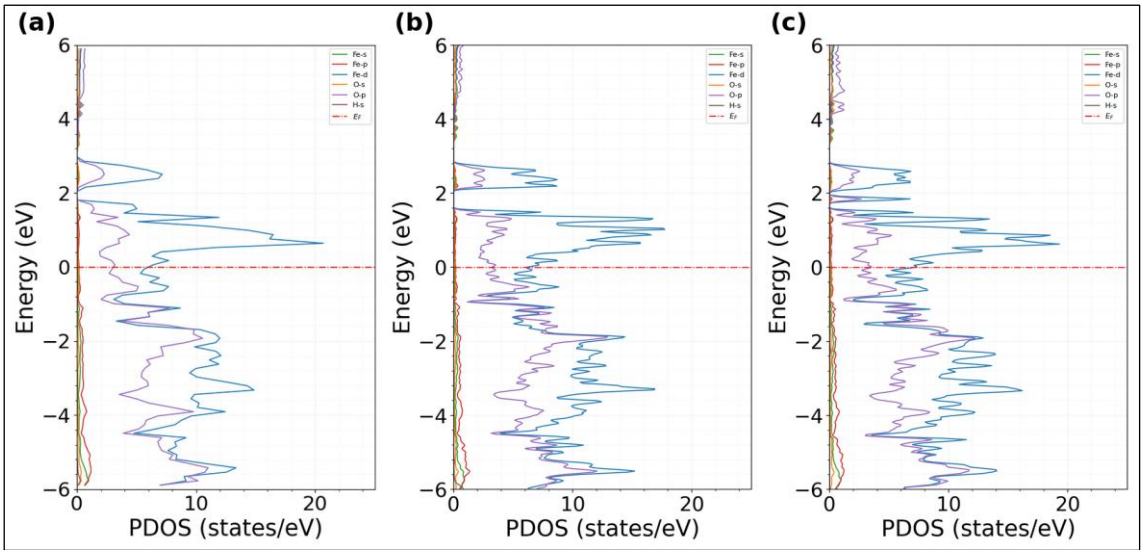


Figure 5. Projected Density of States (PDOS) of the $\alpha - Fe_2O_3$ Surface with Adsorbed (a) $H_2O$, (b) $\bullet OH$ and (c) $\bullet OOH$ at the Fe-top site. The Progressive Broadening of the Fe-3d States Reflects the Increasing Interaction Strength $H_2O < \bullet OH < \bullet OOH$.

Table 2. Summary Of the Computed Electronic and Adsorption Trends.

| System / species | Key computed result | $d_{ads}$ (Å) |
|---|---|---|
| $\alpha - Fe_2O_3$ | Indirect gap 1.28 eV; VB: O-2p, CB: Fe-3d; AFM | - |
| $CuO/Fe_2O_3$ | Indirect gap 1.61 eV (+0.33 eV); Cu-3d/Fe-3d hybridization; Cu-s ~2.8 eV | - |
| $H_2O$ on $Fe_2O_3$ | Weak interaction; O-2p at −1 to −3 eV | 2.255 |
| $\bullet OH$ on $Fe_2O_3$ | Stronger; O-2p nearer E_F; Fe-3d shifts toward E_F | 1.825 |
| $\bullet OOH$ on $Fe_2O_3$ | Strongest; two O-2p peaks; broad Fe-3d (chemisorption) | 1.842 |
| | *Interaction strength order:* $H_2O < \bullet OH < \bullet OOH$. | |

PDOS-based): H₂O < •OH < •OOH. The Fe–O bond distance decreases from 2.26 Å ($H_2O$) to 1.83–1.84 Å (•OH, •OOH).

## CONCLUSION

Spin-polarized DFT+U calculations were used to investigate the electronic structure of α-$Fe_2O_3$, the $CuO/Fe_2O_3$ heterojunction and the adsorption of OER intermediates on the hematite surface. The pristine $\alpha - Fe_2O_3$ slab is an antiferromagnetic semiconductor with an indirect band gap of 1.28 eV, a valence band dominated by O-2p states and a conduction band dominated by Fe-3d states. Forming the $CuO/Fe_2O_3$ heterojunction widens the indirect gap to 1.61 eV (+0.33 eV) through hybridization of Cu-3d and Fe-3d orbitals, with empty Cu-s states appearing near 2.8 eV above the Fermi level. The orbital redistribution evident in the composite

PDOS suggest an S-scheme charge-transfer mechanism, in which CuO and $Fe_2O_3$ act as the reduction and oxidation photocatalysts, respectively. Adsorption of water-derived species follows the interaction order $H_2O$ < $\bullet OH$ < $\bullet OOH$, with $\bullet OOH$ exhibiting the strongest Fe–O hybridization. Together these results indicate the potential of the $CuO/Fe_2O_3$ heterojunction as a candidate visible-light S-scheme photocatalyst for the oxygen evolution reaction in water splitting, with band-alignment, charge-density, and reaction-themodynamics calculation identified as the necessary next steps to substantiate this assignment.

## ACKNOWLEDGEMENT

The authors thank the Department of Physics, Universitas Negeri Padang, for helpful discussions, and Institut Teknologi Bandung for providing the computational resources that supported this work.

## REFERENCES

Alamgir, Mushtaq, N., Ahmad, A., Erum, J. K. E., Li, L., Qian, J., Wang, X., & Gao, J. (2025). Shaping the future of solar-driven photocatalysis by reticular framework materials. *Journal of Materials Science & Technology*, *231*, 193–244. https://doi.org/10.1016/j.jmst.2025.02.009

Blöchl, P. E. (1994). Projector augmented-wave method. *Physical Review. B, Condensed Matter*, *50*(24), 17953–17979. https://doi.org/10.1103/physrevb.50.17953

Dudarev, S., & Botton, G. (1998). Electron-energy-loss spectra and the structural stability of nickel oxide: An LSDA+U study. *Physical Review B - Condensed Matter and Materials Physics*, *57*(3), 1505–1509. https://doi.org/10.1103/PhysRevB.57.1505

Fujishima, A., & Honda, K. (1972). Electrochemical Photolysis of Water at a Semiconductor Electrode. *Nature*, *238*(5358), 37–38. https://doi.org/10.1038/238037a0

Gao, R.-T., Zhang, J., Nakajima, T., He, J., Liu, X., Zhang, X., Wang, L., & Wu, L. (2023). Single-atomic-site platinum steers photogenerated charge carrier lifetime of hematite nanoflakes for photoelectrochemical water splitting. *Nature Communications*, *14*(1), 2640. https://doi.org/10.1038/s41467-023-38343-6

Guo, Y., Tan, X., Yu, T., & Gong, J. (2026). Recent Advances of Photocatalytic Hydrogen Evolution via Water Vapor Splitting. *Advanced Functional Materials*, *36*(17), e22276. https://advanced.onlinelibrary.wiley.com/doi/abs/10.1002/adfm.202522276

Hofmann, O. T., Zojer, E., Hörmann, L., Jeindl, A., & Maurer, R. J. (2021). First-principles calculations of hybrid inorganic-organic interfaces: From state-of-the-art to best practice. *Physical Chemistry Chemical Physics*, *23*(14), 8132–8180. https://doi.org/10.1039/d0cp06605b

Huang, X., Ramadugu, S. K., & Mason, S. E. (2016). Surface-Specific DFT + U Approach Applied to α-Fe2O3(0001). *The Journal of Physical Chemistry C*, *120*(9), 4919–4930. https://doi.org/10.1021/acs.jpcc.5b12144

Jiang, Z., , Zhang, L., & Yu, J. (2023). Research Progress on S-Scheme Heterojunction Photocatalyst. *Journal of the Chinese Ceramic Society*, *51*(1), 73–81. https://doi.org/10.14062/j.issn.0454-5648.20220459

Kresse, G., & Hafner, J. (1993). Ab initio molecular dynamics for liquid metals. *Phys. Rev. B*, *47*(1), 558–561. https://doi.org/10.1103/PhysRevB.47.558

Kyesmen, P. I., Nombona, N., & Diale, M. (2021). Heterojunction of nanostructured α-Fe2O3/CuO for enhancement of photoelectrochemical water splitting. *Journal of Alloys and Compounds*, *863*, 158724. https://www.sciencedirect.com/science/article/pii/S0925838821001316

Low, J., Yu, J., Jaroniec, M., Wageh, S., & Al-Ghamdi, A. A. (2017). Heterojunction Photocatalysts. *Advanced Materials*, *29*(20), 1601694. https://doi.org/https://doi.org/10.1002/adma.201601694

Lv, D., Gao, J., Shao, Y., Wang, Y., Pan, J., Cong, Y., & Lv, S.-W. (2025). Internal electric field triggered charge

redistribution in CuO/Fe(2)O(3) composite to regulate the peroxymonosulfate activation for enhancing the degradation of organic pollutants. *Environmental Pollution (Barking, Essex : 1987)*, *367*, 125618. https://doi.org/10.1016/j.envpol.2024.125618

Monkhorst, H. J., & Pack, J. D. (1976). Special points for Brillouin-zone integrations. *Phys. Rev. B*, *13*(12), 5188–5192. https://doi.org/10.1103/PhysRevB.13.5188

Nallapureddy, R. R., Arla, S. K., Ibáñez, A., Pabba, D. P., Jung, J. H., & Joo, S. W. (2025). Photosensitizer and Charge Separator Roles of g-$C_3N_4$ Integrated into the CuO-$Fe_2O_3$ p-n Heterojunction Interface for Elevating PEC Water Splitting Potential. *Nanomaterials*, *15*(7), 1–16. https://doi.org/10.3390/nano15070551

Naveas, N., Pulido, R., Marini, C., Hernández-Montelongo, J., & Silván, M. M. (2023). First-principles calculations of hematite (α-Fe2O3) by self-consistent DFT+U+V. *IScience*, *26*(2). https://doi.org/10.1016/j.isci.2023.106033

Nørskov, J. K., Rossmeisl, J., Logadottir, A., Lindqvist, L., Kitchin, J. R., Bligaard, T., & Jónsson, H. (2004). Origin of the Overpotential for Oxygen Reduction at a Fuel-Cell Cathode. *The Journal of Physical Chemistry. B*, *108*(46), 17886–17892. https://doi.org/10.1021/jp047349j

Perdew, J. P., Burke, K., & Ernzerhof, M. (1996). Generalized Gradient Approximation Made Simple. *Phys. Rev. Lett.*, *77*(18), 3865–3868. https://doi.org/10.1103/PhysRevLett.77.3865

Sivula, K., Le Formal, F., & Grätzel, M. (2011). Solar Water Splitting: Progress Using Hematite (α-Fe2O3) Photoelectrodes. *ChemSusChem*, *4*(4), 432–449. https://doi.org/https://doi.org/10.1002/cssc.201000416

Tanwar, K., Lo, C., Eng, P., Catalano, J., Walko, D., Brown, G., Waychunas, G., Chaka, A., & Trainor, T. (2007). Surface diffraction study of the hydrated hematite (1-102) surface. *Surface Science*, *601*, 460–474. https://doi.org/10.1016/j.susc.2006.10.021

Walter, M. G., Warren, E. L., McKone, J. R., Boettcher, S. W., Mi, Q., Santori, E. A., & Lewis, N. S. (2010). Solar Water Splitting Cells. *Chemical Reviews*, *110*(11), 6446–6473. https://doi.org/10.1021/cr1002326

Wang, V., Xu, N., Liu, J.-C., Tang, G., & Geng, W.-T. (2021). VASPKIT: A user-friendly interface facilitating high-throughput computing and analysis using VASP code. *Computer Physics Communications*, *267*, 108033. https://doi.org/https://doi.org/10.1016/j.cpc.2021.108033

Xu, Q., Zhang, L., Cheng, B., Fan, J., & Yu, J. (2020). S-Scheme Heterojunction Photocatalyst. *Chem*, *6*(7), 1543–1559. https://doi.org/https://doi.org/10.1016/j.chempr.2020.06.010